Nanotechnology

PAPER • OPEN ACCESS

Intrinsic electron trapping in amorphous oxide

To cite this article: Jack Strand *et al* 2018 *Nanotechnology* **29** 125703

View the article online for updates and enhancements.

Recent citations

- Intrinsic charge trapping in amorphous oxide films: status and challenges
Jack Strand *et al*

IOP ebooks™

Bringing you innovative digital publishing with leading voices to create your essential collection of books in STEM research.

Start exploring the collection - download the first chapter of every title for free.

This content was downloaded from IP address 128.41.35.15 on 07/08/2018 at 14:40

OPEN ACCESS
IOP Publishing

Nanotechnology

Nanotechnology **29** (2018) 125703 (10pp)

https://doi.org/10.1088/1361-6528/aaa77a

Intrinsic electron trapping in amorphous oxide

Jack Strand[1,6], Moloud Kaviani[2], Valeri V Afanas'ev[3], Judit G Lisoni[4] and Alexander L Shluger[2,5]

[1] Department of Physics and Astronomy, University College London, Gower Street, London WC1E 6BT, United Kingdom
[2] WPI-Advanced Institute for Materials Research, Tohoku University, Sendai 980-8577, Japan
[3] Department of Physics, University of Leuven, Celestijnenlaan 200D, 3001 Leuven, Belgium
[4] Institute of Physics and Mathematics, Faculty of Science, Universidad Austral de Chile, Valdivia, Chile and Interuniversity Microelectronics Center (IMEC), 3001 Leuven, Belgium
[5] Department of Physics and Astronomy and London Centre for Nanotechnology, University College London, Gower Street, London WC1E 6BT, United Kingdom

E-mail: jack.strand.14@ucl.ac.uk, moloud.kaviani@gmail.com, valeri.afanasiev@fys.kuleuven.be, judit.lisoni@uach.cl and a.shluger@ucl.ac.uk

Received 3 November 2017, revised 22 December 2017
Accepted for publication 15 January 2018
Published 7 February 2018

Abstract

We demonstrate that electron trapping at intrinsic precursor sites is endemic in non-glass-forming amorphous oxide films. The energy distributions of trapped electron states in ultra-pure prototype amorphous (a)-HfO_2 insulator obtained from exhaustive photo-depopulation experiments demonstrate electron states in the energy range of 2–3 eV below the oxide conduction band. These energy distributions are compared to the results of density functional calculations of a-HfO_2 models of realistic density. The experimental results can be explained by the presence of intrinsic charge trapping sites formed by under-coordinated Hf cations and elongated Hf–O bonds in a-HfO_2. These charge trapping states can capture up to two electrons, forming polarons and bi-polarons. The corresponding trapping sites are different from the dangling-bond type defects responsible for trapping in glass-forming oxides, such as SiO_2, in that the traps are formed without bonds being broken. Furthermore, introduction of hydrogen causes formation of somewhat energetically deeper electron traps when a proton is immobilized next to the trapped electron bi-polaron. The proposed novel mechanism of intrinsic charge trapping in a-HfO_2 represents a new paradigm for charge trapping in a broad class of non-glass-forming amorphous insulators.

Keywords: amorphous HfO_2, exhaustive photo-depopulation spectroscopy, charge trapping, DFT calculations, intrinsic electron traps

(Some figures may appear in colour only in the online journal)

1. Introduction

Thin oxide films grown on various surfaces via oxidation and deposition are ubiquitous in environment and technologies. Their structure is strongly affected by interfaces, and differs from that of bulk materials, resulting in a number of unusual electrical properties [1]. Importantly, such films can grow (poly)-crystalline or amorphous, depending on the deposition and annealing conditions. Amorphous oxide films are used in a broad variety of applications requiring ever reducing oxide thickness combined with mechanical flexibility and reliability. In particular, few-nanometer thin amorphous oxide insulators are attracting significant interest due to their applications enabling electric field control in nano-electronic devices [2–6]. Unlike the SiO_2 traditionally employed in

[6] Author to whom any correspondence should be addressed.

Original content from this work may be used under the terms of the Creative Commons Attribution 3.0 licence. Any further distribution of this work must maintain attribution to the author(s) and the title of the work, journal citation and DOI.

opto- and micro-electronic technologies, most oxides, such as the widely used ZrO_2, HfO_2, Al_2O_3, MgO, ZnO, TiO_2 and In-Ga-Zn-O, are non-glass-formers. Few-nm thick films of these oxides are metastable, and prone to structural changes in the course of technological processing and operation. However, little is still known about how their structure affects the key property of the insulating material required to enable the electric field control, i.e. the ability of the oxide film to remain electrically neutral under bias application and carrier injection conditions. For example, early concerns that leakage current densities may be higher across polycrystalline dielectrics than in amorphous films of the same composition because defective grain boundary regions may enhance electronic conduction [7, 8] prompted wide applications of amorphous films.

The reduced density and disorder in amorphous oxide films both lead to a significant fraction of ions having reduced coordination with respect to bulk crystalline materials [9–13]. Therefore, a much better studied nano-crystalline form of these oxides can provide a fruitful analogy to draw upon for clues regarding the behavior of ultra-thin amorphous films. For example, no electron or hole trapping is observed in the bulk of non-defective crystalline MgO [14]. However, both electrons and holes can be captured at low-coordinated corner and kink sites at surfaces of MgO nano-crystallites, due to the reduced Madelung potential [15]. Electrons and holes form shallow polaron states in the bulk of crystalline ZrO_2, HfO_2 [16, 17] and ZnO [18], but low-coordinated sites at surfaces of these materials form much deeper trapping states [19, 20]. Can the lower coordination of ions in the amorphous phase of such oxides also lead to intrinsic electron or hole trapping in deep states? The results of theoretical calculations of amorphous a-HfO_2 support this hypothesis [21]. However, *proving* the intrinsic nature of electron traps in nm thick amorphous films is challenging, and requires synergy between theory and experiment.

Here, we combine experimental (exhaustive photodepopulation spectroscopy, EPDS, with improved resolution) and theoretical (Time-dependent Density Functional Theory, TD-DFT) methods to demonstrate that electronic gap states responsible for a deep electron trapping in prototype a-HfO_2 insulating films are intrinsic, and originate from lower coordination of ions and elongation of bonds in the amorphous phase of a-HfO_2. HfO_2 films are chosen here due to the availability of synthetic oxide layers of highest purity, which is vital in studying their *intrinsic* properties, and due to their practical importance in microelectronics and in a growing range of other applications. In particular, HfO_2 and $HfSi_xO_y$ are the primary contenders to replace SiO_2 in a variety of nano-electronic devices, ranging from deep-scaled transistors to DRAM [5, 6] and non-volatile memory cells [22, 23], and —in combination with metal gate electrodes—they are already used in the first generation of such devices [24]. We propose that the presence of low-coordinated ions in amorphous oxides with significant *p* and *d* character of electron states near the conduction band bottom (CBB) can lead to similar electron trapping and significantly affect characteristics of nanodevices.

2. Methodology

2.1. Experimental

The experimentally studied samples were prepared by ALD of HfO_2 on thermally oxidized (100)Si wafers by production-grade atomic layer deposition (ALD) process using $HfCl_4$ and H_2O precursors at 300 °C. Thicknesses of SiO_2 and HfO_2 were 7.5 and 20 nm, respectively. Some samples were subsequently annealed for 15 min in N_2 (1 atm) at 1000 °C. Metal-oxide–Si (MOS) capacitors were completed by thermo-resistive evaporation of semi-transparent electrodes (13 nm Au) of 1 mm^2 area on the oxide stack, excluding exposure of the insulating layers to ionizing radiation.

Energy distribution of trap levels in the HfO_2 band gap was determined by using exhaustive photodepopulation spectroscopy (EPDS) which is based on the phenomenon of photoionization (or photodepopulation) of defect states [25–27]. EPDS employs measurements of the insulator charge using capacitance–voltage (CV) curves—and, moreover, allows the photo-depopulation to reach saturation, i.e. to exhaust all charge carriers available for optical excitation at a given photon energy hν. By starting from a low photon energy hν and then increasing it by a small energy step δhν, the saturation of the de-trapping kinetics within each photon energy interval [hν; hν + δ hν] signifies that there is virtually no electron left available for optical transitions to the CBB in this energy window. The amount of charge de-trapped during the next step will then exactly correspond to the density of occupied electron states with energy levels within the energy interval δhν. By performing the EPDS at incremental photon energies one can find the distribution of the electron states across the insulator band gap [25–27]. Compared to previous experiments [28], the modified optical scheme of the excitation source enabled improvement of the energy resolution to 200 meV. As a result, we succeeded in resolving two spectral components of the trapped electron energy distribution discussed below.

EPDS measurements were carried out at room temperature in the spectral range of 1.25 < hν < 6.5 eV, using an energy increment δhν of 0.2 eV (with constant wavelength resolution of 10 nm) under +2 V bias applied to the top metal electrode [28]. The exposure time per step was 1 h, which guarantees removal of at least 90% of charge available for de-trapping at every $h\nu$ as monitored by 200 kHz CV curve measurement.

After analyzing an as-fabricated (pristine) MOS capacitor, the latter was injected with electrons or holes by applying a 20-ms long 'write' voltage pulse to the metal electrode. The pulse amplitude V_g was increased in steps of 1 or 2 V to achieve different trapped-charge densities. Electron injection experiments on the control MOS capacitors with only one layer of 7.5 nm thick SiO_2 insulator (no HfO_2) under the same strength of electric field as in SiO_2/HfO_2 stacks indicate that trapping of negative charge in silicon oxide is negligible. Therefore, the observed electron traps should be located in HfO_2. Upon charging, the capacitors were kept in darkness for 48 h, to allow for completion of thermal

de-trapping before exposure to light starting from the lowest photon energy of 1.25 eV. After each illumination step, the charge variation in the insulating stack was monitored using CV curves. The corresponding charge density ΔQ_{stack} was calculated from the shift of the flatband point assuming uniform distribution of traps across the HfO_2 layer. The latter assumption is supported by the downscaling of the trapped electron density with reducing HfO_2 thickness, as verified by experiments on MOS capacitors with 5 nm thick HfO_2 overlayers. Finally, the spectral charge density (SCD) was calculated by normalizing the density of the re-charged centers to the spectral step width $\delta h\nu$. More detailed description of the measurements can be found in the literature [25–28]. Importantly, all trapped electrons can be removed from the HfO_2 layer in the course of EPDS, indicating that traps analyzed in this study represent the dominant source of electron trapping.

2.2. Computational modeling

To study charging of a-HfO_2 samples, we used the amorphous structures generated and characterized in our previous work [21]. These were produced using classical molecular dynamics and a melt-and-quench procedure. The LAMMPS package [29] was used with a force-field parametrized in [30]. In particular, cubic periodic cells containing 324 atoms were initially equilibrated at 300 K. The temperature was then linearly ramped to 6000 K at constant pressure, and the structures were stabilized for 500 ps at 6000 K. The systems were cooled down from 6000 K to 0 K in 8 ns with a cooling rate of 0.75 K/ps. The Berendsen thermostat and barostat were used to control the simulations. The partially crystallized structures were obtained using a similar method with crystalline seeds included in the melt, as discussed in more detail below.

Further optimization of the volume and geometry of these structures, and calculation of charge trapping sites, were performed using DFT implemented in the CP2K code [31, 32] with the nonlocal PBE0-TC-LRC functional and the exchange cutoff radius of 4.0 Å[32]. The CP2K code employs a Gaussian basis set mixed with an auxiliary plane-wave basis set [33]. Double-ζ Gaussian basis sets [34] were employed on all atoms in conjunction with the GTH pseudopotential [35]. The plane-wave cutoff was set to 6530 eV (480 Ry). To reduce the computational cost of nonlocal functional calculations, the auxiliary density matrix method (ADMM) was employed [32]. All geometry optimizations were performed using the BFGS optimizer to minimize forces on atoms to within 2.3×10^{-2} eV Å^{-1}. The trapping energies of excess electrons and holes were corrected using the method of Lany and Zunger [36, 37] and a dielectric constant of 22 [38]. Optical transition energies were calculated using the Time-dependent Density Functional Theory (TD-DFT) method, as implemented in the CP2K code [39]. Cubic periodic cells containing 324 atoms were used in all calculations.

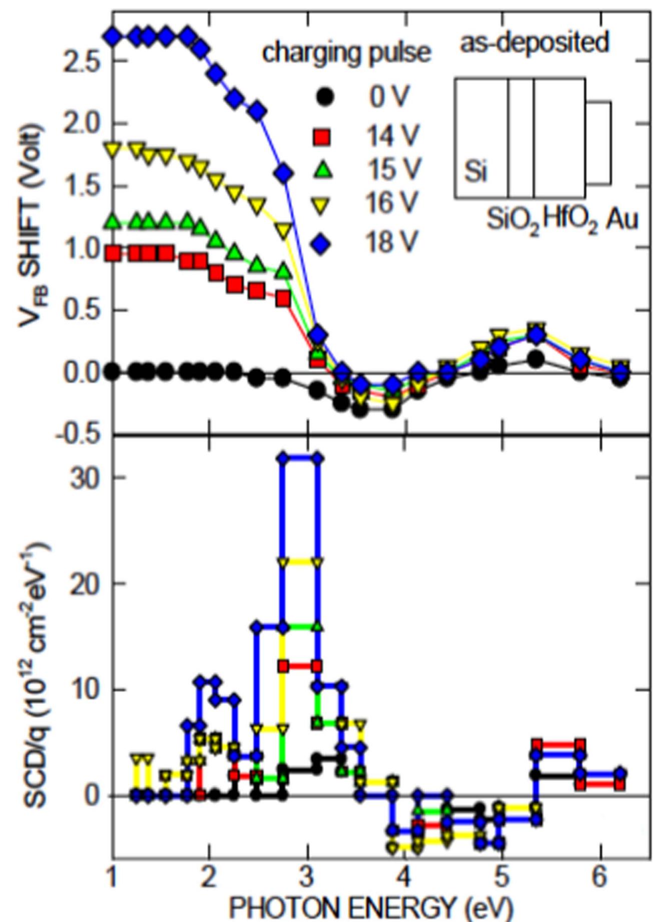

Figure 1. Illumination-induced charge variations (top) and the inferred SCD distributions (bottom) for samples with 19-nm thick HfO_2 insulator in pristine state and after injection of electrons by tunneling out of silicon by applying the charging voltage pulse of the indicated amplitude.

3. Results

3.1. Energy distribution of electron traps

Figures 1 and 3 summarize the major experimental findings of EPDS measurements performed on the pristine and electron-injected samples with as-deposited 19-nm thick HfO_2 insulator ($HfCl_4$+H_2O ALD precursor chemistry; for results on other films see reference [28]). Using the stepwise increase of photon energy $h\nu$ and monitoring of the oxide charge by measuring the shift of flatband voltage (VFB) on 100 kHz capacitance−voltage curve (figure 1, top panel) the illumination-induced charge variation can be converted to the spectral charge density (SCD) (figure 1, bottom panel), which reflects the contributions of the various electron processes to the oxide charging.

One can distinguish three spectral ranges with different electron transitions dominating the charging process [28]. Here, we focus on the spectral region $h\nu < 4$ eV, where electrons are excited from the energy levels E_t in the oxide gap, leading to a slight positive charging in the pristine HfO_2 sample or, otherwise, to the removal of electrons captured in HfO_2 upon electron tunneling. Two important features are

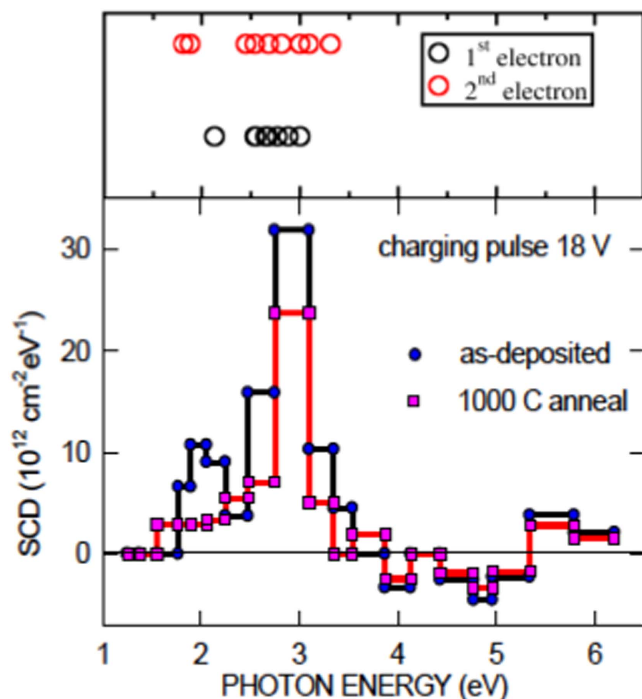

Figure 2. Top panel shows the results of theoretical calculations of polaron and bi-polaron excitation energies to the mobility edge, indicated by hollow circles. Bottom panel compares inferred SCD distribution in the as-deposited sample and in the structure with HfO_2 layer crystallized by a 15 min anneal in N_2 at 1000 °C.

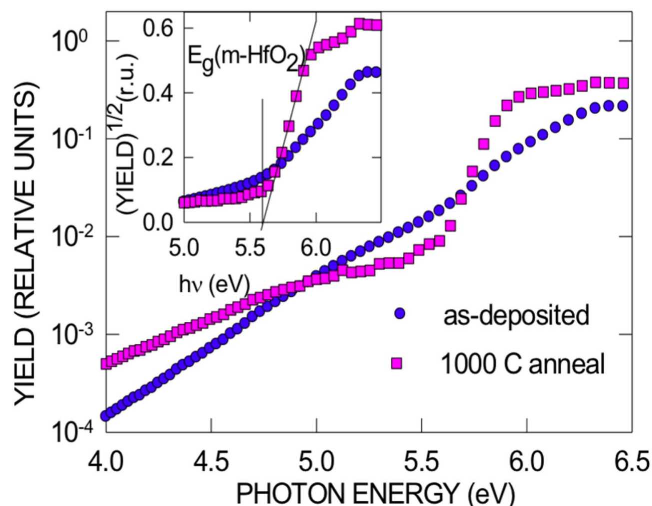

Figure 3. Photo-current yield spectra in the vicinity of the oxide photo-conductivity threshold measured in the as-deposited sample and after a 15 min anneal in N_2 at 1000 °C. The inset illustrates determination of the oxide band gap E_g from the (Yield)$^{\frac{1}{2}}$-hv plot.

worth noting: (1) In the electron-injected samples, nearly all the trapped electrons can be de-trapped under illumination in the spectral range $h\nu < 4$ eV; 2) The charging spectrum of the pristine HfO_2 layer fits in with that of the electron de-trapping, suggesting that the apparent positive charging of the as-deposited a-HfO_2 layer is also due to de-trapping of electrons from acceptor states partially filled by electrons during ALD growth of the oxide. The origin of charge variations induced by illumination with higher energy photons is discussed in detail in [28].

The excitation of electrons from the gap states into the HfO_2 CB represents the dominant (dis)-charging mechanism in the range $h\nu < 4$ eV. Thus the SCD shown in the bottom panel of figure 1 directly reflects the energy distribution of the initial electron states. The spectral plots in figure 1 clearly show that there are at least two components of the trapped electron density—one at $2\,eV < E_t < 3\,eV$ and another one deeper, at $3\,eV < E_t < 3.5$ eV, which have not been resolved previously [28].

To yield further insight into the origin of these electron traps in HfO_2, we examined the effect of annealing which leads to partial crystallization of HfO_2. The structure of annealed samples is discussed in detail in supplementary material and below. Figure 2 compares the SCD spectra obtained on the as-deposited sample and the one subjected to 15 min anneal in N_2 at 1000 °C. Spectral dependence of the photo-conductivity (PC) yield, defined as the photo-current normalized to the incident photon flux, are shown in figure 3 for the as-deposited and annealed HfO_2 films. These curves indicate the spectral threshold of $E_g = 5.6$ eV corresponding to the monoclinic phase of HfO_2 after applying the high-temperature anneal [40]. It should be noted, however, that electron microscopy study (see the supplemental material) demonstrates that the annealed films still contain significant volume fraction of amorphous hafnia. The corresponding photoexcitation threshold (at around 5.9–6.0 eV—see the PC spectra of a-HfO_2 layers on Si_3N_4 [41]) or with admixture of Al, which prevents crystallization [42], can hardly be distinguished on the photo-conductivity spectra shown in figure 3 because it is energetically above that of the crystallized m-HfO_2 PC onset at 5.6 eV. In turn, from the SCD distributions shown in figure 2 one may conclude that the shallow component of the electron trap spectrum is strongly attenuated upon annealing of a-HfO_2. By contrast, deep traps with optical depth of about 3.0 eV remain preserved.

3.2. Theoretical simulations of trapped charge

3.2.1. Geometric structure of a-HfO$_2$. To understand the origin of the observed charging and SCD distributions, we modeled intrinsic charge trapping in a-HfO_2. Using NPT classical molecular dynamics simulations, we produced thirty a-HfO_2 structures with densities of about 9.0 g cm^{-3}, which exhibit wide distributions of bond lengths and atomic coordinations and the existence of two-coordinated O and five-coordinated Hf ions [21]. The atomic structures further optimized using DFT have higher densities, in the range of 9.2–9.9 g cm^{-3}, averaging at 9.6 g cm^{-3}. The average Hf–O bond length is 2.1 Å (ranging from 1.95 to 2.35 Å), very close to the Hf–O bond lengths in m-HfO_2 (around 2.1 Å). In further calculations we study the characteristics of excess

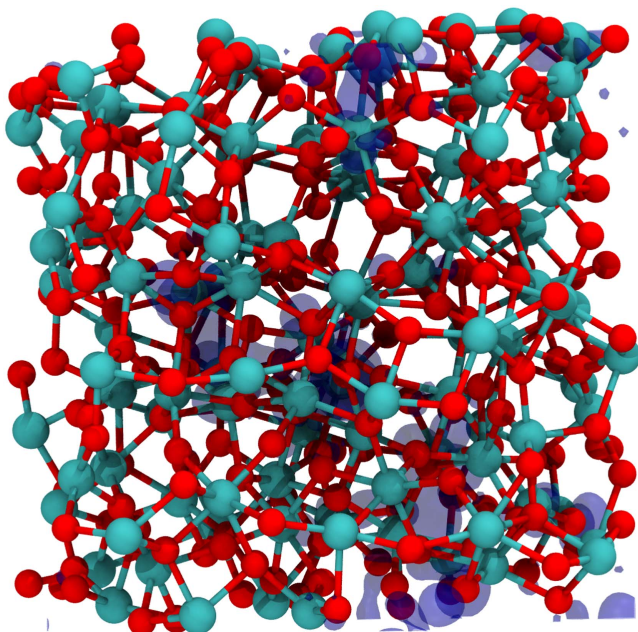

Figure 4. Geometric structure of a disordered periodic cell and iso-surface of the square modulus of the KS state forming the bottom of the conduction band or LUMO state. As can be seen, the LUMO is partially localized.

electrons in ten 324 atom structures with densities in the narrow range of 9.5–9.75 g cm^{-3}.

3.2.2. Electronic structure of a-HfO$_2$. States at both the top of the valence band and the bottom of the conduction band of a-HfO_2 are characterized by the partial localization onto oxygen 2*p* and hafnium 5*d* electronic states, respectively (see figure 4). The degree of localization of these states was further analyzed by calculating the inverse participation ratio (IPR) spectrum. This method takes advantage of the atom-centered basis set used in CP2K to quantify the degree of localization of each eigenvector. It has often been used to characterize localization of vibrational and electronic states in amorphous solids (see e.g. [43–47]). Specifically, if the Kohn–Sham (KS) states are linear combinations of atom-centered basis functions, $\psi_n(\mathbf{r}) = \sum_i^N c_{ni}\phi_i(\mathbf{r})$, where ϕ_i are the basis functions, the IPR can be calculated as:

$$\mathrm{IPR}(\psi_n) = \frac{\sum_i^N c_{ni}^4}{\left(\sum_i^N c_{ni}^2\right)^2}. \quad (1)$$

The IPR was calculated for each KS state in the valence band and conduction band. In this definition, IPR ranges between 0 and 1, and is very small for a delocalized KS orbital. For example, for a state fully delocalized across all basis functions with all of the coefficients of its basis functions equal to one another, the IPR will be $\mathrm{IPR}(\psi_n) = \frac{1}{N}$, N being the total number of basis functions. Alternatively, localized KS orbitals will have high-valued IPRs.

A typical IPR spectrum of a-HfO_2 is shown in figure 5. One can see that there are localized states both at the CBB and at the top of the valence band of a-HfO_2. The latter lead to

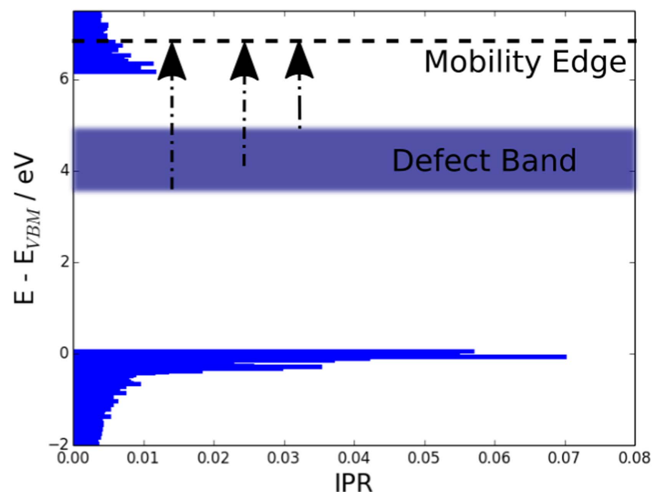

Figure 5. Typical IPR spectrum of the a-HfO_2 valence and conduction bands. The spectrum is taken from a typical cell with an electron bi-polaron. Large IPR values at the band edges indicate localization of the state, and small IPR values correspond to delocalized states. The mobility edge position is estimated from the IPR spectrum. The position of the defect band of polarons and bi-polarons is also shown.

hole trapping, as discussed in reference [21]. The IPR for delocalized states in the valence band has a value between 0.003 and 0.0035. This corresponds to delocalization over approximately 300 basis functions. The delocalized states in the conduction band have a slightly higher IPR value of 0.004, due to the lower number of Hf ions in the system.

3.2.3. Polaron states. Structural disorder serves as a source of 'precursors' for the formation of deep electron states [21]. Precursor sites are associated with the already-localized molecular orbitals at the band edges (as plotted in figure 5). The high IPR valued molecular orbitals are found to be localized onto certain structural motifs, e.g. under-coordinated Hf ions or Hf ions with elongated Hf–O bonds, both of which are associated with a lowering of the electrostatic potential (for an electron). This is shown in figure 6 by plotting the Hartree potential as a function of the radial distance, R, from precursor and normal (non-precursor) Hf ions. The potential is represented at each distance R by averaging over the surface of a sphere of radius R, centered on the respective ion. This is repeated for a sample of precursor ions and a sample of normal ions, and an average is taken for each. As one can see in figure 6, the Hartree potential experienced by an electron near precursor sites is on average deeper than at 'regular' Hf sites in a-HfO_2, which makes them more favorable for electron localization. The calculation shows that injected electrons trap onto these precursor sites without needing to overcome an activation barrier. We call these trapped-charge states 'polarons' for brevity, and in analogy with electron polarons in m-HfO_2 which are trapped only by the lattice polarization. In a-HfO_2, however, the electron trapping is facilitated by precursor sites and relaxation of their local environment. In an electron polaron, a single electron is strongly localized over 2 or 3 Hf ions (figure 7). Upon polaron

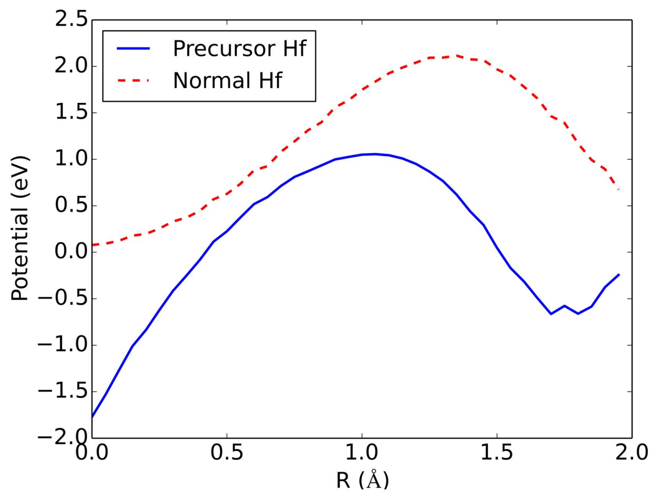

Figure 6. Hartree potential (electrons + ions) as a function of radial distance from Hf ions. The potential shown is the potential as experienced by an electron and shows that precursor Hf ions have a lower (more negative) interaction potential. This helps to localize injected electrons onto precursor sites.

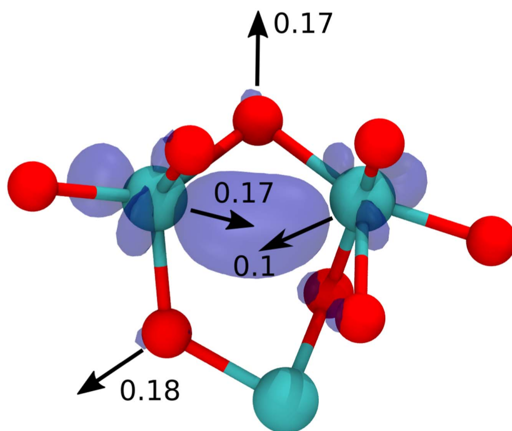

Figure 7. The electron polaron. Blue iso-surfaces indicate the electron density of the polaron state. Red spheres indicate oxygen ions and cyan spheres indicate hafnium ions. Black arrows show the directions of ionic displacements; their values are given in Å.

formation, the Hf_O bonds of these Hf ions are stretched outwards by 0.12 Å averaged over ten configurations. Multiple configurations of polarons were analyzed, and the occupied KS states were found to be distributed between 1.6 and 2.5 eV below the bottom of the conduction band. These states can trap a second electron to form bi-polaron states (figure 8). The second electron is trapped over the same Hf ions, and so the bi-polarons show a similar distribution of electron density to the polarons. The bi-polaron formation is associated with further Hf −O bond stretching of, on average, 0.09 Å. Polaron and bi-polaron states form a band of KS states, as shown in figure 5. The width of this band is determined by the distribution of local environments of precursor sites in the samples of similar density.

3.2.4. Calculated spectral charge density. The electrons photo-ionized from the trap states in the gap are collected at the gate

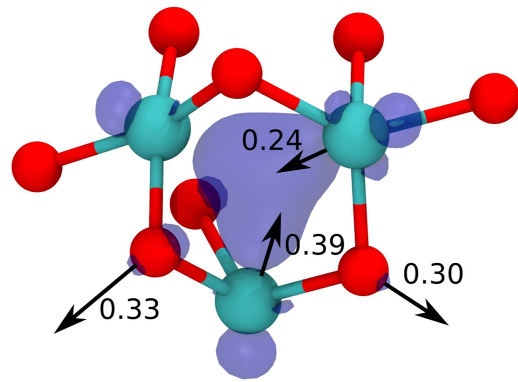

Figure 8. The electron bi-polaron. Blue iso-surfaces indicate the electron density of the bi-polaron state. Red spheres indicate oxygen ions and cyan spheres indicate hafnium ions. Black arrows show the directions of ionic displacements; their values are given in Å.

electrode, and should be mobile. Therefore, to compare with the experimental SCD data shown in figure 2, one needs to calculate a distribution of optical transition energies from polaron and bi-polaron states into the states at or above the electron mobility edge (ME) in the conduction band of a-HfO_2, as illustrated in figure 5. The mobility edge is usually defined as a critical point where there is a transition between localized states—which do not contribute to the electrical conductivity of the system, and extended states—which can contribute to the electrical conductivity in disordered systems [48–50]. Using IPR analysis, one can define ME as the onset of states with an IPR corresponding to delocalized states. At room temperature, this definition is inevitably blurred by thermal activation of conductivity in partially localized states at the edge [49, 50]. We find the ME for electrons in the conduction band to be approximately 0.5 eV above the LUMO KS state (figure 5). It may be expected, given that the transition from localised to delocalized states is gradual, that there is some degree of arbitrariness in placing the mobility edge. We find that the onset of the delocalized states could be plausibly placed 0.1 eV either way, and that this does not significantly affect our results. Further, partially localized states which sometimes appear beyond the mobility edge are usually isolated, and do not affect our definition of ME.

Optical transitions from the charge trapping states into the conduction band were calculated using the TD-DFT method as implemented in the CP2K code [39]. Calculating transitions for polaron configurations in all a-HfO_2 structures is too computationally expensive. Therefore, we first performed TD-DFT calculations for single and bi-polaron configurations in three such structures. These include transitions into the localized states at the bottom of the CB and into the delocalized states above the ME. The TD-DFT calculations show that the energies of electron transitions into the localized states at the bottom of the conduction band are about 0.5 eV smaller than the corresponding KS energy differences due to the electron−hole interaction. However, those into the delocalized states at and above ME are similar to the differences between the corresponding KS energies. This is characteristic of transitions into delocalized states (see

e.g. [51]). Therefore, the optical transitions for other a-HfO_2 structures can be approximated by KS energy differences between the occupied trap state and ME. The mobility edge is calculated for each a-HfO_2 structureu, and is typically found to be around 0.5 eV above the CBB. The distribution of energies shown in figure 2 corresponds to that of KS polaron and bi-polaron states with respect to the corresponding ME, and agrees very well with the experimental spectrum. The intensities of the experimental peaks are determined mainly by the population of the corresponding trap states, which our statistics does not provide.

The agreement of the distribution of the calculated depopulation energies with the experimental SCD suggests that polarons and bi-polarons are likely candidates to explain the negative charging of a-HfO_2 films. To check the consistency of this model with other experimental data, we investigated how thermal annealing affects the behavior of these traps.

3.3. Modeling the annealed samples

A detailed description of experimental observations of the structure of annealed samples is given in the supplementary material. A combination of transmission and scanning electron microscopies and grazing incidence x-ray diffraction on test structures of 25 nm thick oxide layers annealed at 1000 ℃ shows that the amorphous phase most probably remains present in HfO_2 films in significant volume fraction after the anneal. We should note that thinner HfO_2 layers or those deposited using carbon-containing precursors are more resistant to crystallization, and may remain amorphous even at higher thermal budgets. For example, sub-2 nm layers are commonly used as gate insulators in devices attempting to attain the equivalent oxide thickness below 0.5 nm [6].

3.3.1. Modeling partially crystallized HfO_2 samples. To create partially crystallized (pc) structures, we used the same procedure as described above, but a small part of the structure was frozen at perfect cubic HfO_2 lattice sites during both melt and quench (see the supplementary material). For smaller nuclei sizes, a significant part of the structure remains amorphous, and the rest is crystallized (see figure 9). The topology of pc-HfO_2 models obtained using classical MD simulations does not change significantly after full optimization with DFT. They have higher densities than the a-HfO_2 structures, ranging from 9.8 to 10.2 g cm^{-3}. One structure of each density has been chosen to perform further calculations. These structures are described in more detail in the supplementary material. The band gap of pc-HfO_2 structures does not contain localized states due to the under-coordinated atoms and is equal to 6.0 eV on average. The IPR spectrum (see the supplementary material) is similar to that of the a-HfO_2 cells, and exhibits localization at the band edges and a conduction band ME approximately 0.5 eV above the CBB.

As in the case of a-HfO_2, we observe spontaneous localization of polarons and bi-polarons in deep states in each of the considered systems. However, the number of precursor

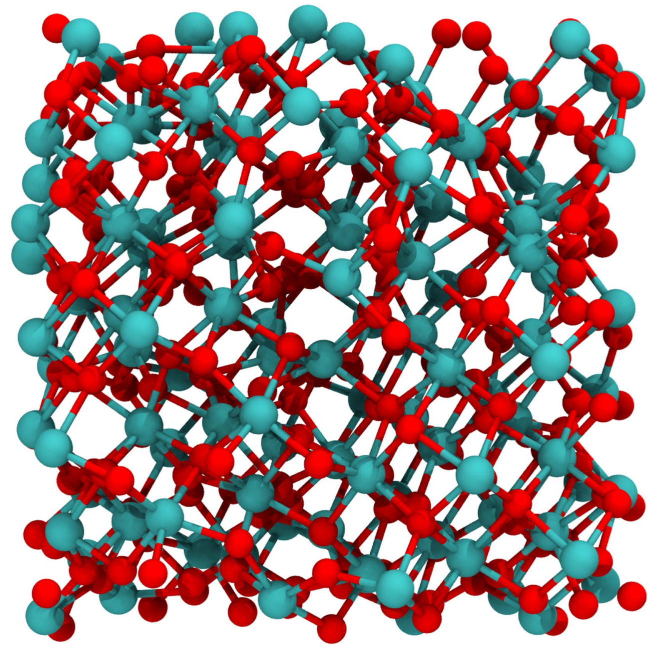

Figure 9. Geometric structure of a partially crystallized disordered periodic cell of HfO_2.

sites is reduced, as they are confined to the disordered regions in the structure. Further DFT calculations show that the crystal phases of HfO_2 either have very shallow polarons (monoclinic, tetragonal), or do not facilitate trapping at all (e.g. bulk cubic). The formation of relatively shallow electron polarons has been predicted in monoclinic HfO_2 in reference [16].

The extra electron(s) in pc-HfO_2 localize on the Hf atoms with six or seven O coordination. Among these, at least three oxygen neighbors have Hf–O distances longer than 2.16 Å. Extra electron(s) can also be localized on five-coordinated Hf atoms, which have longer Hf–O bonds. The average position of the KS level for the electron polaron in these structures is 2.4 eV below the bottom of the conduction band, whereas for bi-polarons it is 2.3 eV below the bottom of the conduction band. More than 90% of the electron spin density is localized on two Hf ions. The TD-DFT calculations of electronic excitations for several bi-electron structures show similar excitation energies to those reported in figure 2. Thus, the anneal changes the SCD by reducing the number of available electron trapping sites.

In addition, annealing can release hydrogen present at the interface as a result of the growth method, and also from metal electrodes. This hydrogen can interact with electron traps, or create further traps [52]. Experimentally, the electron injection is performed after the anneal, which can promote proton diffusion into pc-HfO_2. Therefore, we first considered five–seven different configurations of protons near the electron trapping precursor sites in the amorphous part of pc-HfO_2 structures, and optimized their geometries. Extra electrons were then localized at precursor sites, to simulate single and bi-electron trapping. The neutral extra electron + proton configurations were not observed experimentally, as only negatively charged states were monitored. Similarly to

reference [52], we observed that in some configurations the proton reacted spontaneously with trapped electron(s), forming an interstitial H^0 atom or H^- ion. In metastable configurations of a proton near a bi-electron trap, the KS level is shifted by about 0.1 eV. Thus, release of protons from the interface can further reduce the charge density, but does not significantly affect the energies of trapped electrons.

4. Discussion and conclusions

To summarize, our experimental and theoretical results provide the first significant evidence of intrinsic electron trapping in amorphous oxide films. Using ultra-pure HfO_2 films, we demonstrate that electron injection leads to formation of localized states with energies about 2–3.5 eV below the mobility edge in the conduction band. The DFT calculations demonstrate that single and bi-electrons trapped at structural precursor sites in a-HfO_2 are likely candidates to explain the charge trapping. High-temperature annealing of the films leads to their partial crystallization, but amorphous regions still remain. DFT calculations demonstrate that electrons trapped in these regions have similar properties to those in amorphous samples, albeit a lower number of precursor sites. The interaction of trapped electrons with protons, which can be released from the interface during annealing, further reduces the number of traps. These results consistently explain the nature of charge trapping in HfO_2 films revealed by EPDS spectra. The agreement of the experimental spectra with theoretical models suggests that low-coordinated ions in amorphous oxides can serve as deep electron traps in oxide films.

Developing reliable methods to identify and analyze electron traps in thin films is of utmost importance in eliminating or limiting their impact on the performance of a growing range of HfO_2 based devices. For example, it has recently been suggested that ferroelectricity of both doped [53, 54] and pure [55] HfO_2 may offer paths to further applications of HfO_2 films, including memories [56] and high sub-threshold slope transistors [57]. However, the positive bias-temperature instability driven by electron injection into oxide films limits the gate oxide scaling in metal$-HfO_2-$Si transistors [24, 58–60]. Furthermore, in flash cells, electron trapping in the integrated HfO_2 insulator degrades the program/erase window, retention and endurance [61, 62].

Besides their importance in improving the performance of a-HfO_2 films, our results should be seen in a broader context, because variability of the cation coordination represents an intrinsic property of many other amorphous oxides [9–13], as well as nano-crystallites widely used in photocatalysis. In particular, electrons in oxides with p and d character of CBB often have low dispersion, and are particularly prone to charge localization. But electrons and holes can behave very differently in the bulk and at surfaces of these materials. A good example is TiO_2, where electron polarons are very shallow in the bulk [63] but much deeper at surfaces and in nanocrystals, where the atomic coordination is lower and bonds are strained [64, 65]. Therefore, one may expect this mechanism of electron trapping to be relevant to a broad variety of other non-glass-forming insulating oxides. By contrast, electrons in s states (e.g. ZnO [66] and Al_2O_3 [67]) have higher dispersion, and are likely to remain mobile even in the amorphous phase [68].

Acknowledgments

MK and ALS are grateful to the World Premier International Research Center Initiative (WPI) sponsored by the Ministry of Education, Culture, Sports, Science and Technology (MEXT), Japan for financial support. ALS acknowledges funding provided by EPSRC under grant EP/K01739X/1. Computer facilities on Archer service have been provided via the UK's HPC Materials Chemistry Consortium (EPSRC Grant No. EP/L000202). The authors thank the Supercomputer Center, the Institute for Solid State Physics, the University of Tokyo for the facilities and the use of the SGI Altix ICE 8400EX. The authors are grateful A-M El-Sayed, D Z Gao and O Dicks for helpful discussions.

ORCID iDs

Jack Strand https://orcid.org/0000-0002-4603-6151

References

[1] Dearnaley G, Stoneham A M and Morgan D V 1970 Electrical phenomena in amorphous oxide films *Rep. Prog. Phys.* **33** 1129

[2] Wilk G D, Wallace R M and Anthony J M 2001 High-κ gate dielectrics: Current status and materials properties considerations *J. App. Phys.* **89** 5243–75

[3] Schlom D G, Guha S and Datta S 2008 Gate oxides beyond SiO_2 *MRS Bull.* **33** 1017–25

[4] Kittl J A *et al* 2009 High-k dielectrics and metal gates for future generation memory devices *ECS Trans.* **19** 29–40

[5] Clark R D 2014 Emerging applications for high-κ materials in VLSI technology *Materials* **7** 2913–44

[6] Robertson J and Wallace R M 2015 High-k materials and metal gates for CMOS applications *Mater. Sci. Eng. Rep.* **88** 1–41

[7] Kim H, McIntyre P C and Saraswat K C 2003 Effects of crystallization on the electrical properties of ultrathin HfO_2 dielectrics grown by atomic layer deposition *Appl. Phys. Lett.* **82** 106–8

[8] Bersuker G *et al* 2011 Grain boundary-driven leakage path formation in HfO_2 dielectrics *Solid-State Electron.* **65** 146–50

[9] Lamparter P and Kniep R 1997 Structure of amorphous Al_2O_3 *Phys. B: Cond. Matt.* **234** 405–6

[10] Lee S K, Lee S B, Park S Y, Yi Y S and Ahn C W 2009 Structure of amorphous aluminum oxide *Phys. Rev. Lett.* **103** 095501

[11] Davis S and Gutiérrez G 2011 Structural, elastic, vibrational and electronic properties of amorphous Al_2O_3 from *ab initio* calculations *J. Phys.: Cond. Matt.* **23** 495401

[12] Buchholz D B, Ma Q, Alducin D, Ponce A, Jose-Yacaman M, Khanal R, Medvedeva J E and Chang R P H 2014 The structure and properties of amorphous indium oxide *Chem. Mater.* **26** 5401–11

[13] Petkov V, Holzhüter G, Tröge U, Gerber T and Himmel B 1998 Atomic-scale structure of amorphous TiO_2 by electron, x-ray diffraction and reverse monte carlo simulations *J. Non-Cryst. Solids* **231** 17–30

[14] Lushchik A, Lushchik C, Nagirnyi V, Pazylbek S, Sidletskiy O, Schwartz K, Shablonin E, Shugai A and Vasil'chenko E 2013 On the mechanisms of radiation damage and prospects of their suppression in complex metal oxides *Phys. Status Solidi* B **250** 261–70

[15] Sterrer M, Diwald O, Knözinger E, Sushko P V and Shluger A L 2002 Energies and dynamics of photoinduced electron and hole processes on MgO powders *J. Phys. Chem.* B **106** 12478–82

[16] Ramo D M, Shluger A L, Gavartin J L and Bersuker G 2007 Theoretical prediction of intrinsic self-trapping of electrons and holes in monoclinic HfO_2 *Phys. Rev. Lett.* **99** 155504

[17] McKenna K P, Wolf M J, Shluger A L, Lany S and Zunger A 2012 Two-dimensional polaronic behavior in the binary oxides m-HfO_2 and m-ZrO_2 *Phys. Rev. Lett.* **108** 116403

[18] Sezen H *et al* 2015 Evidence for photogenerated intermediate hole polarons in ZnO *Nature Commun.* **6** 6901

[19] Wolf M J, McKenna K P and Shluger A L 2012 Hole trapping at surfaces of m-ZrO_2 and m-HfO_2 nanocrystals *J. Phys. Chem.* C **116** 25888–97

[20] van Dijken A, Meulenkamp E A, Vanmaekelbergh D and Meijerink A 2000 The kinetics of the radiative and nonradiative processes in nanocrystalline ZnO particles upon photoexcitation *J. Phys. Chem.* B **104** 1715–23

[21] Kaviani M, Strand J, Afanas'ev V V and Shluger A L 2016 Deep electron and hole polarons and bipolarons in amorphous oxide *Phys. Rev.* B **94** 020103

[22] Molas G *et al* 2009 Reliability of charge trapping memories with high-κ control dielectrics *Microelectron. Eng.* **86** 1796–803

[23] Breuil L, Lisoni J G, Blomme P, Van den Bosch G and Van Houdt J 2014 HfO_2 base high-κ inter-gate dielectrics for planar NAND flash memory *IEEE Electron Device Lett* **35** 45–7

[24] Ando T 2012 Ultimate scaling of high-κ gate dielectrics: Higher-κ or interfacial layer scavenging? *Materials* **5** 478–500

[25] Afanas'ev V V, Wang W C, Cerbu F, Madia O, Houssa M and Stesmans A 2014 (Invited) Spectroscopy of deep gap states in high-k insulators *ECS Trans.* **64** 17–22

[26] Wang W-C, Badylevich M, Afanas'ev V V, Stesmans A, Adelmann C, Elshocht S Van, Kittl J A, Lukosius M, Walczyk C and Wenger C 2009 Band alignment and electron traps in Y_2O_3 layers on (100) Si *Appl. Phys. Lett.* **95** 132903

[27] Zahid M B, Aguado D R, Degraeve R, Wang W-C, Govoreanu B, Toledano-Luque M, Afanasev V V and Houdt J V 2010 Applying complementary trap characterisation technique to crystalline γ-phase-Al_2O_3 for improved understanding of nonvolatile memory operation and reliability *IEEE Trans. Electron Devices* **57** 2907–16

[28] Cerbu F *et al* 2016 Intrinsic electron traps in atomic-layer deposited HfO_2 insulators *Appl. Phys. Lett.* **108** 222901

[29] Plimpton S 1995 Fast parallel algorithms for short-range molecular dynamics *J. Comput. Phys.* **117** 1–19

[30] Broglia G, Ori G, Larcher L and Montorsi M 2014 Molecular dynamics simulation of amorphous HfO_2 for resistive RAM applications *Model. Simul. Mater. Sci. Eng.* **22** 065006

[31] VandeVondele J, Krack M, Mohamed F, Parrinello M, Chassaing T and Hutter J 2005 Quickstep: Fast and accurate density functional calculations using a mixed Gaussian and plane waves approach *Comput. Phys. Commun.* **167** 103–28

[32] Guidon M, Hutter J and VandeVondele J 2009 Robust periodic Hartree–Fock exchange for large-scale simulations using Gaussian basis sets *J. Chem. Theory Comput.* **5** 3010–21

[33] Lippert G, Hutter J and Parrinello M 1997 A hybrid Gaussian and plane wave density functional scheme *Mol. Phys.* **92** 477–88

[34] VandeVondele J and Hutter J 2007 Gaussian basis sets for accurate calculations on molecular systems in gas and condensed phases *J. Chem. Phys.* **127** 114105

[35] Goedecker S, Teter M and Hutter J 1996 Separable dual-space Gaussian pseudopotentials *Phys. Rev.* B **54** 1703–10

[36] Lany S and Zunger A 2009 Accurate prediction of defect properties in density functional supercell calculations *Model. Simul. Mater. Sci. Eng.* **17** 084002

[37] Lany S and Zunger A 2008 Assessment of correction methods for the band-gap problem and for finite-size effects in supercell defect calculations: Case studies for ZnO and GaAs *Phys. Rev.* B **78** 235104

[38] Driemeier C, Wallace R M and Baumvol I J 2007 Oxygen species in HfO_2 films: an *in situ* x-ray photoelectron spectroscopy study *J. App. Phys.* **102** 024112

[39] Iannuzzi M, Chassaing T, Wallman T and Hutter J 2005 Ground and excited state density functional calculations with the Gaussian and augmented-plane-wave method *CHIMIA Int. J. Chem.* **59** 499–503

[40] Hoppe E E and Aita C R 2008 Suppression of near-edge optical absorption band in sputter deposited HfO_2-Al_2O_3 nanolaminates containing nonmonoclinic HfO_2 *Appl. Phys. Lett.* **92** 141912

[41] Afanas'ev V V and Stesmans A 2007 Internal photoemission at interfaces of high-κ insulators with semiconductors and metals *J. Appl. Phys.* **102** 081301

[42] Afanasev V V, Stesmans A and Tsai W 2003 Determination of interface energy band diagram between (100) Si and mixed Al-Hf oxides using internal electron photoemission *Appl. Phys. Lett.* **82** 245–7

[43] Bell R J and Dean P 1970 Atomic vibrations in vitreous silica *Discuss. Faraday Soc.* **50** 55–61

[44] Chang T-M, Bauer J D and Skinner J L 1990 Critical exponents for Anderson localization *J. Chem. Phys.* **93** 8973–82

[45] Dong J and Drabold D A 1996 Band-tail states and the localized-to-extended transition in amorphous diamond *Phys. Rev.* B **54** 10284

[46] Drabold D A, Stephan U, Dong J and Nakhmanson S M 1999 The structure of electronic states in amorphous silicon *J. Mol. Graphics Modell* **17** 285–91

[47] Unge M and Christen T 2014 Electron and hole mobility edges in polyethylene from material simulations *Chem. Phys. Lett.* **613** 15–8

[48] Youn Y, Kang Y and Han S 2014 An efficient method to generate amorphous structures based on local geometry *Comput. Mater. Sci.* **95** 256–62

[49] Anderson P W 1972 The size of localized states near the mobility edge *Proc. Nat. Acad. Sci. U. S. A* **69** 1097–9

[50] Mott N 1987 The mobility edge since 1967 *J. Phys.* C **20** 3075

[51] Izmaylov A F and Scuseria G E 2008 Why are time-dependent density functional theory excitations in solids equal to band structure energy gaps for semilocal functionals, and how does nonlocal Hartree-Fock-type exchange introduce excitonic effects? *J. Chem. Phys.* **129** 034101

[52] Kaviani M, Afanas'ev V V and Shluger A L 2017 Interactions of hydrogen with amorphous hafnium oxide *Phys. Rev.* B **95** 075117

[53] Park M H *et al* 2015 Ferroelectricity and antiferroelectricity of doped thin HfO_2-based films *Adv. Mater.* **27** 1811–31

[54] Böscke T S, Müller J, Bräuhaus D, Schröder U and Böttger U 2011 Ferroelectricity in hafnium oxide thin films *Appl. Phys. Lett.* **99** 102903

[55] Polakowski P and Müller J 2015 Ferroelectricity in undoped hafnium oxide *Appl. Phys. Lett.* **106** 232905

[56] Müller J, Polakowski P, Müller S and Mikolajick T 2015 Ferroelectric hafnium oxide based materials and devices: Assessment of current status and future prospects *ECS J. Solid State Sci. Technol.* **4** N30–5
[57] Karda K, Jain A, Mouli C and Alam M A 2015 An anti-ferroelectric gated landau transistor to achieve sub-60 mv/dec switching at low voltage and high speed *Appl. Phys. Lett.* **106** 163501
[58] Kerber A and Cartier E A 2009 Reliability challenges for CMOS technology qualifications with hafnium oxide/titanium nitride gate stacks *IEEE Trans. Device Mater. Reliab.* **9** 147–62
[59] Cartier E *et al* 2011 Fundamental aspects of HfO_2-based high-k metal gate stack reliability and implications on tinv-scaling *Electronic Devices Meeting (IEDM), 2011 IEEE Int.* pp 18–24
[60] Ioannou D P and CMOS H K M G 2014 technology qualification: The PBTI reliability challenge *Microelectron. Reliab.* **54** 1489–99
[61] Govoreanu B, Degraeve R, Zahid M B, Nyns L, Cho M, Kaczer B, Jurczak M, Kittl J A and Houdt J V 2009 Understanding the potential and limitations of HfAlO as interpoly dielectric in floating-gate flash memory *Microelectron. Eng.* **86** 1807–11
[62] Zahid M B, Degraeve R, Breuil L, Blomme P, Lisoni J G, Van den Bosch G, Houdt J V and Tang B J 2014 Defects characterization of hybrid floating gate/inter-gate dielectric interface in flash memory *Reliability Physics Symp., 2014 IEEE Int.* 2E–3 IEEE
[63] Yang S *et al* 2013 Intrinsic small polarons in rutile TiO_2 *Phys. Rev.* B **87** 125201
[64] Dimitrijevic N M, Saponjic Z V, Rabatic B M, Poluektov O G and Rajh T 2007 Effect of size and shape of nanocrystalline TiO_2 on photogenerated charges. An epr study *J. Phys. Chem.* C **111** 14597–601
[65] Chiesa M, Paganini M C, Livraghi S and Giamello E 2013 Charge trapping in TiO_2 polymorphs as seen by electron paramagnetic resonance spectroscopy *Phys. Chemist. Chem. Phys.* **15** 9435–47
[66] Erhart P, Albe K and Klein A 2006 First-principles study of intrinsic point defects in zno: Role of band structure, volume relaxation, and finite-size effects *Phys. Rev.* B **73** 205203
[67] Sabino F P, Besse R, Oliveira L N, Wei S-H and Da Silva J L F 2015 Origin of and tuning the optical and fundamental band gaps in transparent conducting oxides: The case of M_2O_3 (M = Al, Ga, In) *Phys. Rev.* B **92** 205308
[68] Dicks O and Shluger A 2017 Theoretical modeling of charge trapping in crystalline and amorphous Al_2O_3 *J. Phys.: Cond. Matt.* **29** 314005